Surface and Coatings Technology, Volume 428, December 2021, Article number 127900
DOI:10.1016/j.surfcoat.2021.127900

Rapid surface finishing of chemical vapour deposited tungsten carbide hard coatings by electropolishing

Christian Micallef[1,2], Cheng-Wei Chiu[1], Yuri Zhuk[2], and Adrianus Indrat Aria[1,*]

[1] Surface Engineering and Precision Institute, School of Aerospace, Transport and Manufacturing, Cranfield University, Cranfield MK43 0AL, United Kingdom; A.I.Aria@cranfield.ac.uk, ORCID: 0000-0002-6305-3906; C.Micallef@cranfield.ac.uk, ORCID: 0000-0003-0409-9573; C.Chiu@cranfield.ac.uk
[2] Hardide Coatings Plc, Bicester OX26 5AH, United Kingdom; yzhuk@hardide.com
[*] Corresponding author: A.I.Aria@cranfield.ac.uk

Abstract

Tungsten/tungsten carbide (W/WC) coatings deposited through chemical vapour deposition (CVD) exhibit favourable mechanical properties and are widely used to extend the working life and performance of engineering parts which operate in high wear and corrosive environments. Following the coating deposition process, the coated parts must adhere to low surface roughness and geometrical tolerance specifications necessitating the need of a machining or surface finishing operation. Unlike monolithic materials, hard W/WC coatings have low machinability due to their high hardness and superior mechanical properties. In this study, electropolishing, which is independent of the material's hardness and capable of processing parts with complex geometries has been studied as a prospective noncontact machining and surface finishing technique for CVD W/WC coatings. Here we report the electropolishing behaviour of W/WC coatings with an average thickness of 50 ± 15 µm and 1300 ± 50 HV hardness. Optimal electropolishing parameters using 5 wt% sodium hydroxide (NaOH) electrolyte concentration at 21 °C allow a mirror-like surface finish with Ra of less than 50 nm and a change in coating thickness of up to 18 µm to be achieved within 5 mins. The change in electrolyte temperature from 21 °C to 40 °C was found to have a significant effect on the electropolishing behaviour due to the formation of a thin and unstable viscous film. The electrolyte concertation of 5 wt% was more stable when compare to 3 wt%, giving an overall better surface finish. EBSD analysis revealed that grains with a {111} orientation were preferentially etched in NaOH.

Keywords: electropolishing, tungsten carbide, chemical vapour deposition, surface finish

Introduction

Tungsten carbide (WC) is an advanced technical ceramic with superior mechanical properties, such as high hardness, stiffness, and wear resistance, along with exceptional physicochemical characteristics, such as high melting point and corrosion resistance [1–4]. WC is highly suitable for use as tribological coatings in a wide range of engineering applications where extreme resistance to wear and corrosion is paramount to extend the usable lifetime of critical components [5,6]. Typical applications include pumps and valves handling abrasive fluids such as quartz, gravel and sand [7], aerospace components subjected to abrasive, adhesive and fretting wear [8], and plastic extrusion dies where the operating temperatures can exceed 400 °C [9]. Apart from providing enhanced protection to the substrate materials, the surface condition of the coatings typically requires conformity to low surface roughness and stringent geometrical tolerance specifications. This leads to the requirement of post-production machining and surface finishing operations [10], typically in a form of mechanical surface finishing

Published by Elsevier. This is the Author Accepted Manuscript issued with: Creative Commons Attribution Non-Commercial No Derivatives License (CC:BY:NC:ND 4.0).
The final published version (version of record) is available online at DOI:10.1016/j.surfcoat.2021.127900. Please refer to any applicable publisher terms of use.

techniques such as grinding, honing, and superfinishing [11,12]. However, the superior mechanical and physicochemical properties of WC coatings make their machinability challenging and time consuming. As WC coatings have the potential to replace existing hard coatings with adverse health effect, e.g. hard chromium coatings from hexavalent chromium, it is imperative to further the understanding of techniques and parameters for machining and surface finishing of WC coatings [13].

The WC coatings considered in this work are deposited through chemical vapour deposition (CVD). CVD is a versatile vapour-phase process that is commonly used for synthesis of advanced materials including multi-length scale low-dimensional materials [14–16], optical and electronic thin films [17,18], and hard coatings [5,19]. The non-line-of-sight nature of CVD makes it ideal for coating deposition on parts with complex and intricate geometries, such as internal cavities and sharp corners. Nonetheless, such complex features often obstruct mechanical machining process and thus satisfactory surface finish can be difficult to achieve. Electropolishing is an attractive surface finishing technique for this reason, as it allows processing of parts with complex geometries and is independent of the material's hardness [20].

To date, research work into the electropolishing of WC coatings is largely scarce with a limited body of literature focusing on the electropolishing of cemented carbide coatings [21–24]. It is important to note that the composition and thus properties of cemented carbide coatings are significantly different to those of the CVD WC coatings studied herein due to the presence of heterogeneous structure composed of hard WC micro-grains, with typical size of several microns across, within the much softer cobalt (Co) or Nickel (Ni) metal binders [25,26]. In contrast, our CVD WC coatings are binder-free and pore-free, as they have a homogeneous composite structure composed of WC nanoparticles dispersed in a hard tungsten (W) metal matrix [5,27] (Supporting information Figure SI 1). The homogeneity of the CVD tungsten/tungsten carbide (W/WC) coatings allows the application of electrochemical approaches, which have been thus far limited to metallurgical W, on the W/WC coatings considered in this work [28–30].

In this work, we report a rapid electropolishing of W/WC coatings where a mirror-like surface finish with an average Ra of less than 50 nm was achieved within 5 mins using a sodium hydroxide (NaOH) electrolyte. NaOH is widely used in the extraction and recovery of W where the chemical mechanisms involved in the dissolution of tungsten are well established [28,31–33]. W dissolution occurs under anodic potentials, in alkaline solutions such as NaOH where W transforms into tungstate ions (WO_4^2). This behaviour is outlined in the Pourbaix diagram where material dissolution occurs at a pH range of 5 to 14 (Supporting information Figure SI 2) [34]. We systematically investigate the electropolishing parameter space using various electrolyte concentrations, electrolyte temperatures, variable potential regimes, and inter-electrode gap widths. Our findings demonstrate the effectiveness of electropolishing as a noncontact machining technique to provide geometrical size corrections and optimal surface finishing conditions for CVD W/WC coatings. Our approach and analysis offer insights into surface finishing of other hard coatings and difficult to process materials for the benefit of many engineering applications.

Experimental Procedure

In this study, samples were in a form of flat rectangular coupons of 35 x 50 mm cut from a commercial-grade 304 stainless steel sheet of 3 mm thickness. The samples were mechanically roughened with a

P80 grit abrasive paper and then cleaned in an ultrasonic bath and degreased in perchloroethylene. Tungsten/tungsten carbide (W/WC) coating was deposited by Hardide Coatings Ltd. (Bicester, Oxford-UK) on these stainless-steel coupons using chemical vapour deposition (CVD) at a temperature of 500 ^{o}C. The metal matrix composite coating is crystallized from gas media atom-by-atom and is composed of nanostructured tungsten carbide particles dispersed in a tungsten metal matrix [5,11]. It is free from inter-granular inclusions, impurities, porosity, and other defects. W/WC coatings with thickness of 50 ± 15 µm and hardness of 1300 HV were used herein.

The electropolishing was carried out in a flat bottom crystallising dish with a 19 cm diameter. The W/WC coated coupon was electrically connected to the anode whilst a copper plate was used as the cathode (Supporting information Figure SI 3). The sample was partially immersed in the electrolyte solution, leaving the top end of the samples (15 mm) in the as-deposited condition to be used as a baseline reference to change in coating characteristics following the process. A surface area of about 21 cm^2 was exposed to the electrolyte solution during testing. The input voltage was supplied through an adjustable DC power supply (0-30VDC/0-20A). The current behaviour was then measured indirectly through a Hall effect current transducer (LTSR 25-NP, LEM UK) while the output voltage was recorded through an oscilloscope (PicoScope 2000 series). An Ag/AgCl electrode was used as the reference electrode. Sodium hydroxide (NaOH, Fischer Scientific UK) was used as the electrolyte for all electrochemical studies. The solution was prepared from 16 wt% NaOH and diluted using deionised water to 5 wt% and 3 wt% concentrations, with pH of 12.8 and 12.5 respectively. A 1000 ml of electrolyte solution was used for each test.

Potentiodynamic voltage sweeps were carried out at 21 °C using 3 wt % and 5 wt % NaOH electrolytes to study the effect of the electrolyte concentration on the electropolishing behaviour. Based on the current density vs potential behaviour of these tests, potentiostatic tests were then carried out to study the effect of time on the electropolishing behaviour. The effect of electrolyte temperature was studied by conducting tests using 5 wt% electrolyte concertation at temperatures of 21 ^{o}C and 40 ^{o}C. The effect of inter-electrode gaps was studied at room temperatures at both 3 wt% and 5 wt% concentrations using 3, 5 and 15 cm gaps between the workpiece and the copper cathode.

The surface morphology was characterised by scanning electron microscope (SEM, Tescan Vega). Preferential grain etching was determined through electron backscattered diffraction (EBSD, Oxford Instruments). A 3D non-contact surface profiler system with a 20x objective and a sampling scale of 900 x 900 µm was used to characterise the surface roughness of the samples (Taylor Hobson). The data sets were levelled with a Gaussian filter with an L filter nesting index of 0.8 mm. The Ra was used as the main parameter which provides an indication of the change in surface roughness as a consequence of electropolishing. Atomic force microscopy (AFM, Digital Instruments) with a silicon scanning probe with scan surface area of 60 x 60 µm^2 was used to characterise the 3D surface topography of the samples in the as-deposited and electropolished conditions. Electrochemical impedance spectroscopy (EIS) was carried out on the as-deposited and electropolished samples with 5 wt% NaOH using a potentiostat (VERSAstat 4) at a potential of −0.71 V and −0.61 V vs Ag/AgCl, respectively, and a potential modulation of 10 mV. EIS data was collected at a frequency range of 100 k – 100 mHz with 20 frequency points per decade. Data fitting to equivalent circuit model was performed with simplex regression algorithm, which was selected for minimising the sensitivity to initial estimation of the parameters [35], for 100k iterations.

Results

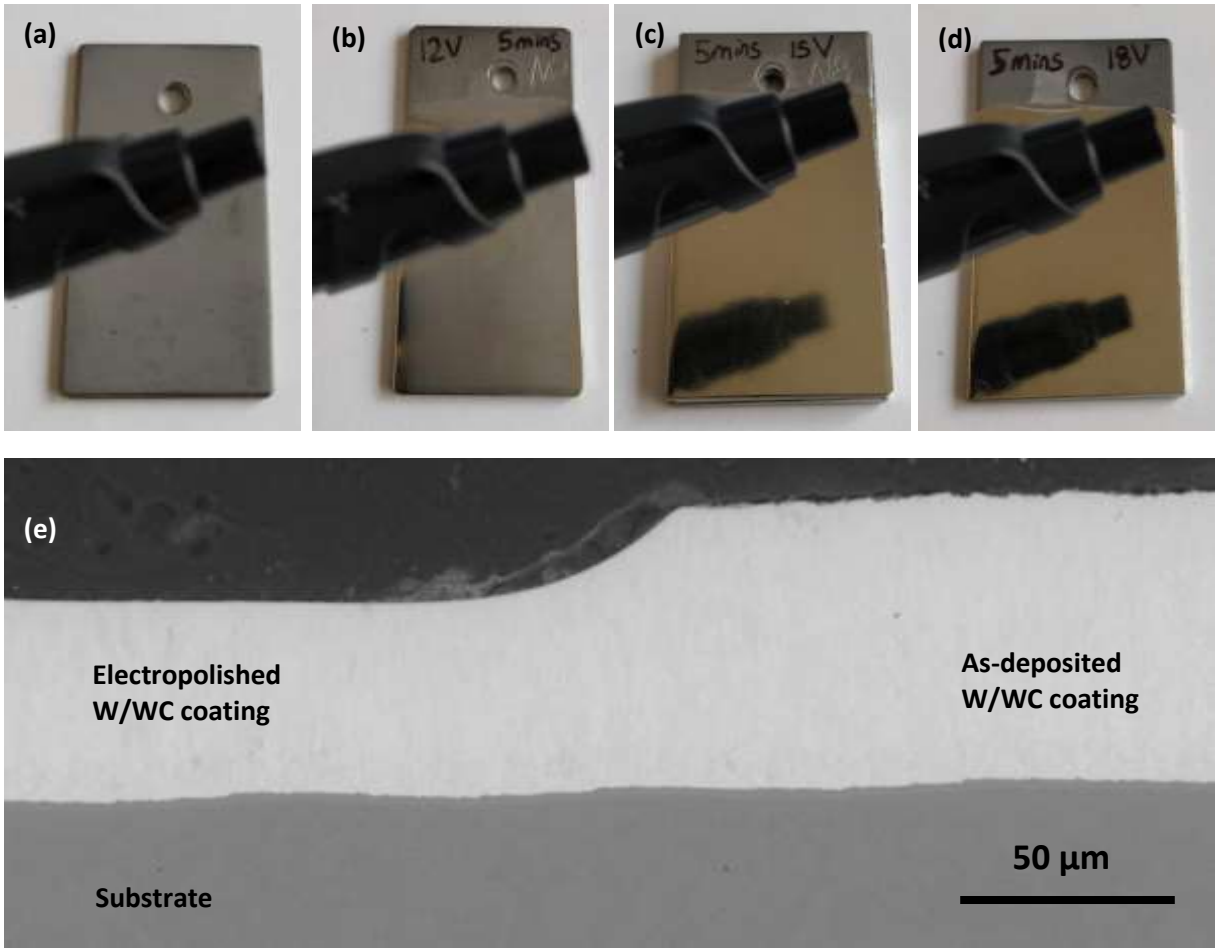


Figure 1: (a-d) Photograph of W/WC coated samples showing the evolution in surface reflection from (a) the matte surface texture of as-deposited W/WC coating to increasingly glossy texture after electropolishing for 5 mins in 5 wt% NaOH at 21 ^{o}C at (b) 4 V, (c) 5.6 V, and (d) 7 V vs Ag/AgCl. (e) Cross-sectional SEM image showing the change in thickness and surface morphology of W/WC coating after being electropolished for 5 mins in 5 wt% NaOH at 7 V vs Ag/AgCl.

The effect of electropolishing to surface finish of W/WC coatings can be visually observed from the evolution in surface reflection. The as-deposited W/WC coating exhibits a matte surface texture (**Figure *1*a**) and a glossier surface texture with improved specular reflectivity can be obtained by electropolishing at a higher applied potential (**Figure *1*b-d**). At a potential of 3.1 V vs Ag/AgCl the development of some surface smoothening around the sample edges becomes visible, although the surface became discoloured. A similar behaviour was observed at a potential of 4 V vs Ag/AgCl , as the sample still exhibit a relatively matte surface texture with some discolouration (**Figure *1*b**). A significant change in surface roughness starts to occur at a potential of 5.5 V vs Ag/AgCl where a much glossier surface texture can be observed (**Figure *1*c**). A mirror-like specular reflection can be observed when the electropolishing is carried out at 7 and 7.9 V vs Ag/AgCl (**Figure *1*d**). Surface smoothening can be observed immediately after the potential is applied with surface smoothening becomes more intense with time for up to a duration of 5 mins. Such a specular reflection can be directly attributed to a smooth surface topography, as observed in the cross-sectional SEM image of the electropolished samples (**Figure *1*e**). The electropolished section of the W/WC coating exhibit a much smoother surface topography compared to the as-deposited section. Note that the electropolishing process also results in a reduction in coating thickness, where about 18 µm of W/WC materials are removed from

the coating in just 5 mins of electropolishing in 5 wt% NaOH at 7 V vs Ag/AgCl. The materials removal rate is found to be increasing with the increase of applied potential in the etching and passivation regimes. In contrast, it is relatively constant in the electropolishing regime (Supporting information Figure SI 4).

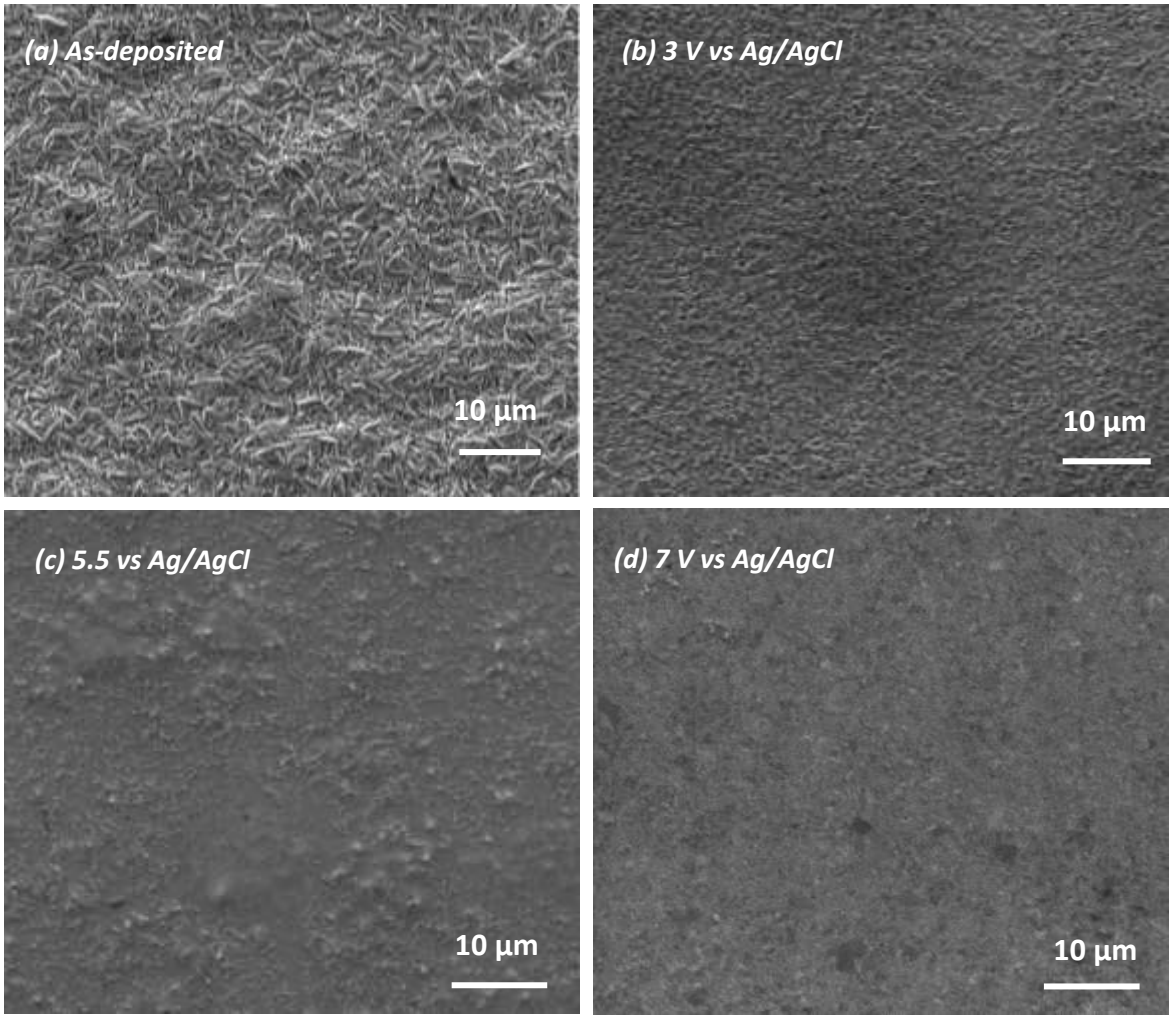


Figure 2: Top view SEM images showing surface morphologies of W/WC coatings (a) as-deposited and after being subjected to electropolishing for 5 mins in 1000 ml of 5 wt% NaOH electrolyte solution at 21 °C at (b) 3 V, (c) 5.5 V, and (d) 7 V vs Ag/AgCl.

The successive improvement in the microscopic surface morphology of the coating as a function of applied electropolishing potential can be observed from the evolution in SEM surface images (**Figure *2*a-d**) and AFM surface scans (**Figure 3a-d**). The as-deposited W/WC coating exhibit a surface morphology with distinctive microstructures and grain boundaries (Supporting information Figure SI 5). These surface features are typical on CVD W/WC coatings due to the microcrystalline growth of metallic W matrix at elevated temperatures [36–38]. AFM surface scans indicate that the as-deposited W/WC coatings have a relatively high surface roughness with Ra of 0.30–0.45 µm (**Figure *3*a**). Electropolishing of W/WC coating at a potential of 3 V vs Ag/AgCl results in the formation of valleys resembling etch pits (**Figure *2*b**). The increase in electropolishing duration from 5 to 10 mins does not result in an improvement in the surface topography of the coating, but only contributes to an increase in the pitting formed on the surface due to a prolonged etching duration. An improvement in the surface topography can be observed at a potential of 5.5 V vs Ag/AgCl, where after 5 mins the surface becomes relatively smooth without any obvious sign of etch pits (**Figure *2*c**). At this potential the

preferential etching of certain grains diminished with a uniform anodic dissolution across the whole surface.

Optimal electropolishing effects are observed at a potential of 7–7.9 V vs Ag/AgCl, where a mirror-like surface finish can be obtained with Ra of 22 nm (**Figure *1*d**). Electropolishing at 7 V vs Ag/AgCl for 5 mins results in a completely clear surface revealing the grain microstructure of the W/WC coating (**Figure 2d**). This sample is virtually flat with the absence of any peaks and valleys with Ra of 22–47 nm (**Figure *3*d**). A similar behaviour can be observed at a potential of 7.9 V vs Ag/AgCl for 2 mins where the grain microstructure was similarly revealed and became clearer when the treatment duration was increased to 5 mins. In agreement with previous studies reported in literature [39,40], the surface roughness decreases progressively with the increase in electropolishing potential irrespective of the initial surface roughness of the coatings (**Figure *3*e**). A coating removal rate of 3.56–3.66 µm/minute was recorded for samples electropolished with 7 V and 7.9 V vs Ag/AgCl potential, respectively (Supporting Information Fig SI 5).

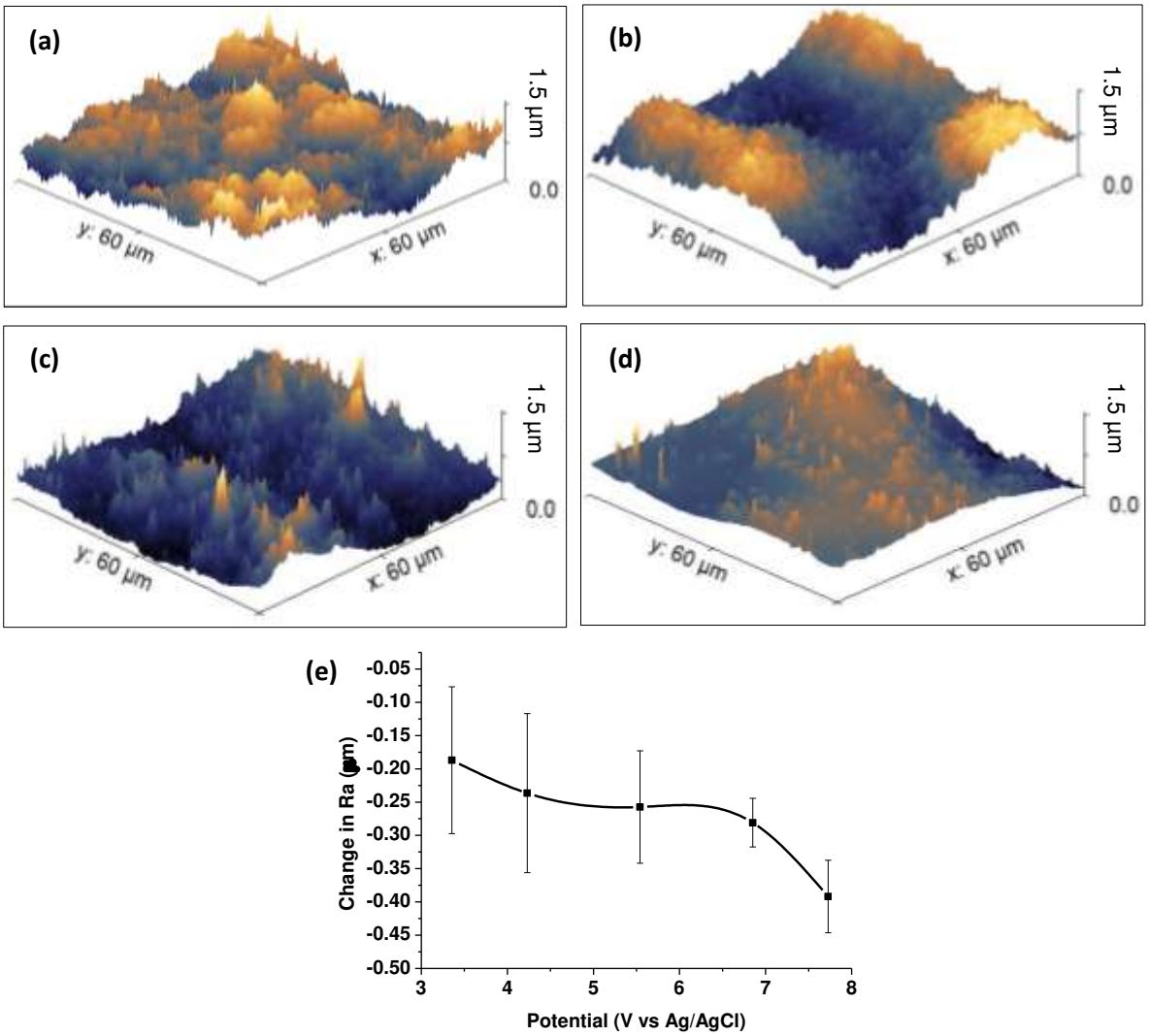


Figure 3: AFM Surface profiles of W/WC coated samples in the (a) as-deposited and electropolished conditions at (b) 3 V vs Ag/AgCl, (c) 5.5 V vs Ag/AgCl and (d) 7.9 V vs Ag/AgCl. (e) Changes in the mean Ra of electropolished W/WC-coated samples vs applied potential vs Ag/AgCl. Zero change in Ra represents the as-deposited condition. The electropolishing conditions for (b)-(e) are 1000 ml of 5 wt% NaOH electrolyte solution at 21 ^{o}C for 5 mins. Error bars represent the uncertainties of the measured data.

Surface EBSD maps reveal the preferential removal on specific microcrystalline grain orientation of W/WC coatings by electropolishing in 5 wt% NaOH. Prior to EBSD analysis, the as-deposited W/WC coating is mechanically polished using colloidal silica to achieve a mirror-like finish without altering their microcrystalline grain orientation. Most microcrystalline grains of mechanically polished W/WC coating are found to exhibit {001} (red) and {111} (blue) planes with a composition of 62% and 34% respectively, while only about 4% of the microcrystalline grains exhibit {101} (green) plane (**Figure *4*a**). In contrast, the microcrystalline grain orientation of electropolished W/WC coating is found to be homogeneous, with 92% of the grains exhibits {001} plane and the remaining 8% exhibits {101} plane (**Figure *4*b**). The disappearance of microcrystalline grains with orientation near {111} plane suggests that they are preferentially etched first during the electropolishing process. In agreement with previous studies, grains with {111} plane are electrochemically more active than those with different orientations and therefore more susceptible to etching in alkaline environment [41–43] It is important to note that the selective removal of grains with {111} orientation does not significantly affect the functionality of the W/WC coatings. The electropolished W/WC coatings are observed to exhibit a hardness of 1264±6.6 HV, which is ~95% of the hardness of as-deposited W/WC at 1331±5.5 HV.

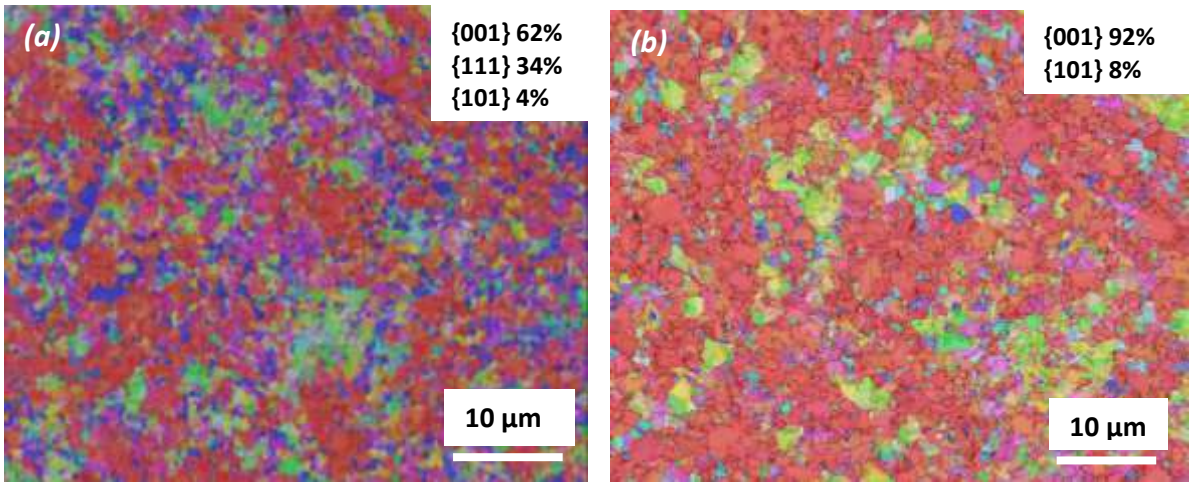


Figure 4: Surface EBSD orientation maps of W/WC coating surface after being (a) mechanically polished using colloidal silica and (b) electropolished in 5 wt% NaOH at 7 V vs Ag/AgCl for 30 s. The mechanically polished W/WC coating exhibits grain distribution of 62% {001}, 34% {111}, and 4% {101}, while the electropolished one exhibits grain distribution of 92% {001} and 8% {101}.

Discussion

As described above, our SEM and AFM analysis indicates that the electropolishing conditions of 7 V vs Ag/AgCl for 5 mins or 7.9 V vs Ag/AgCl for 2 mins in 5 wt% NaOH are optimal to minimise the surface roughness of W/WC coatings. This motivates us to further confirm the decrease in surface roughness by electrochemical impedance spectroscopy (EIS) analysis. The EIS Nyquist (**Figure 5a-b**) plot of the as-deposited sample shows the presence of two distinctive impedance behaviours from the high frequency interaction at the electrode-electrolyte interface and the low frequency response within the electrodes. These behaviours, however, are much less distinctive in the electropolished sample. In the high frequency regime of 100 kHz – 100 Hz, the angle between the imaginary positive part of the impedance (-Zim>0) and the real axis is observed to be between $\pi/4$ and $\pi/2$, suggesting a constant phase element (CPE) impedance behaviour. Interestingly, the Bode plots (**Figure 5c**) shown that the impedance magnitude and phase angle (**Figure 5d**) of both as-deposited and electropolished samples are relatively similar in this high frequency regime. In contrast, the differences in impedance

magnitude and phase angle between these two samples are more pronounced in the low frequency regime of 100 Hz – 100 mHz. In this frequency regime, the impedance magnitude for electropolished sample is consistently lower than that for as-deposited sample. This suggests that the Helmholtz and diffuse viscous layers formed on the surface of electropolished sample are thinner than those on as-deposited sample, which can be attributed to the reduced surface disorder [44–49]. In agreement to the previously reported behaviour on nitride- and oxide-based coatings [50,51], the effect of electropolishing on W/WC coating can be further described by an equivalent circuit with two time constants.

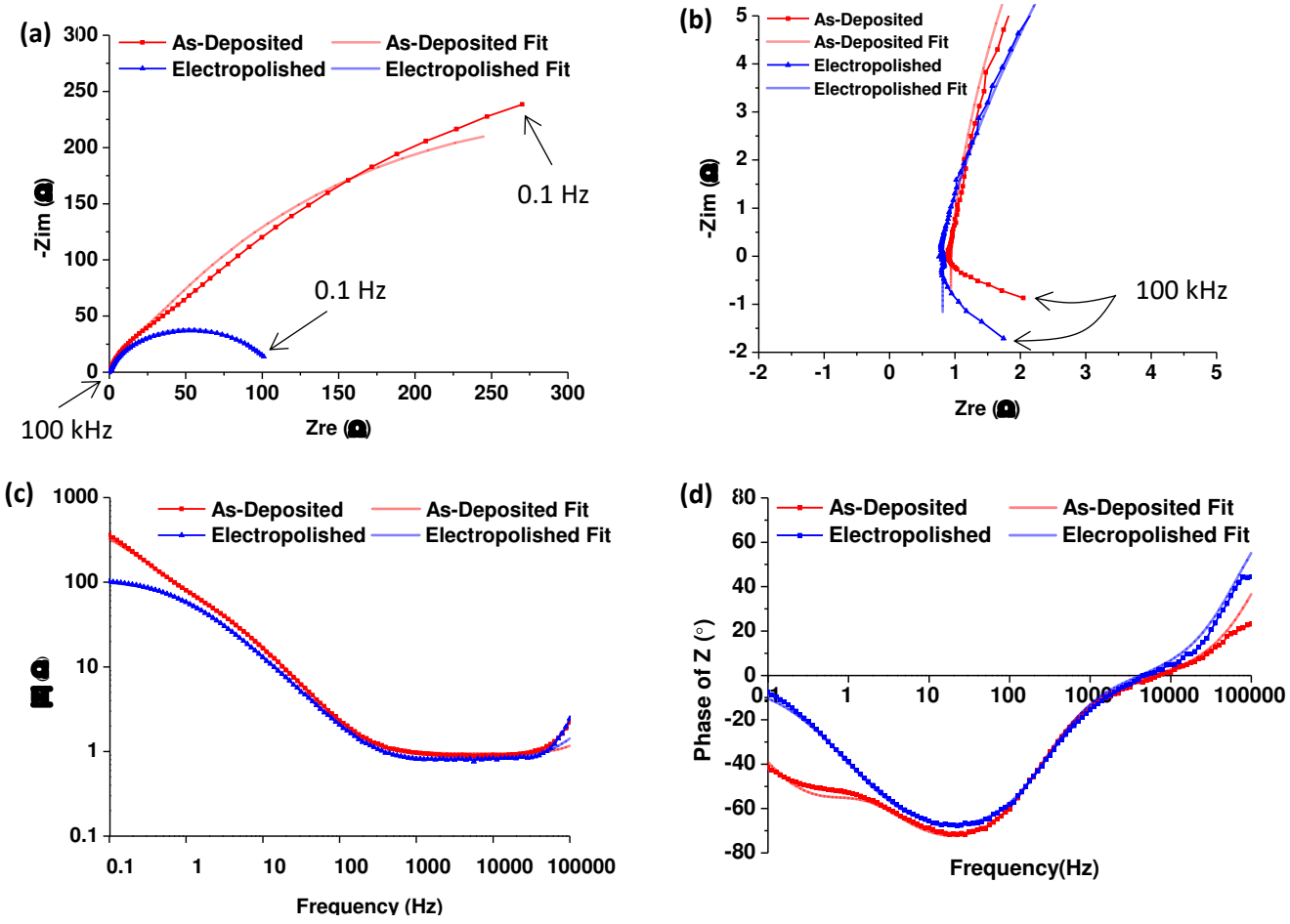


Figure 5: (a) Overall and (b) zoomed-in EIS Nyquist plot, (c) Bode plot and (d) Phase angle vs. log frequency of as-deposited and electropolished W/WC samples obtained at a potential of −0.71 V and −0.61 V vs Ag/AgCl, respectively. Here the samples were electropolished in 5 wt% NaOH with a potential of 7 V vs Ag/AgCl for 2 mins

Here, we fit the EIS data to a fitting model of $L_s + R_s + CPE_{dl}/(R_{ct} + CPE_{ad}/R_{ad})$ (Supporting information Figure SI 6), which is commonly used for electroactive chemical reactions in presence of adsorbed species [35,52–54]. L_s represents the series inductive loss from the electrical connections, wires, and instrument. R_s is the total series resistance of the measurement system with contributions from the ohmic resistances of the electrolyte and the electrodes. CPE_{dl} is the double layer CPE with characteristics parameters of Q_{dl} and α_{dl}. CPE_{ad} is the adsorption CPE with characteristics parameters of Q_{ad} and α_{ad}. R_{ct} and R_{ad} are the charge transfer and adsorption resistances, respectively. Both CPE_{dl} and R_{ct} represent the high frequency response at the electrolyte-electrode interface, while CPE_{ad} and R_{ad} represent the low frequency response from the mass transport within the electrode. EIS data fit analysis (**Table *1***) shows that α_{dl} of as-deposited sample is ~0.93, while that

of electropolished sample is 1. As CPE in the high frequency regime is highly influenced by surface disorder, the $\alpha_{dl} < 1$ of the as-deposited sample suggests a rough and porous surface with heterogeneous reaction sites. In contrast, the $\alpha_{dl} = 1$ of the electropolished sample suggests a smooth and planar surface with homogeneous reaction sites [45–49,54,55]. Interestingly, R_{ct} of as-deposited sample is ~1834 Ω cm^2, which is more than 20 times larger than that of electropolished sample at ~80.35 Ω cm^2. Here, the decrease in R_{ct} is not originated from an increase in surface porosity and roughness [56,57], but rather from a removal of charge barrier layer on the surface of W/WC coating. Note that tungsten oxide (WO_x) layer naturally forms on the surface of W matrix, especially in the presence of an alkaline solution [32,33,58]. This WO_x layer acts as a charge transfer barrier in the as-deposited condition, which is then removed through dissolution into tungstate (WO_4^{2-}) ions during the electropolishing process.

Table 1: EIS data obtained by equivalent circuit simulation of as-deposited and electropolished samples in 5wt% NaOH solution at room temperature.

Constants		As-Deposited	Electropolished (18V, 2mins)	Units
L_s	Series inductance	23.51	39.37	$\mu\mathrm{H}\ cm^2$
R_s	Series resistance	19.82	17.24	$\Omega\ cm^2$
Q_{dl}	Double layer constants	25.55	16.28	$m\mathrm{F}\ s^{\alpha_{dl}-1}\ cm^{-2}$
α_{dl}		0.93	1	
R_{ct}	Charge transfer resistance	1834.01	80.35	$\Omega\ cm^2$
Q_{ad}	Adsorption constants	56.46	50.07	$mF\ s^{\alpha_{ad}-1}\ cm^{-2}$
α_{ad}		0.84	0.66	
R_{ad}	Adsorption resistance	9815.60	2209.04	$\Omega\ cm^2$
χ^2	Goodness of fit	0.93	0.58	

The removal of oxide barrier layer along with a decrease in thickness of W/WC coating by electropolishing process also result in a reduction in resistance to adsorption and diffusion of electroactive species. Note that the electropolishing process at 7 V vs Ag/AgCl for 2 mins reduces the overall thickness of W/WC coating by ~7.2 µm, which is about 12% of the original thickness. In addition to a decrease in coating thickness, the decrease in R_{ad} by a factor of four from ~9815.6 Ω cm^2 for as-deposited sample to ~2209 Ω cm^2 for electropolished sample suggests a continuous increase in the number of adsorption and diffusion sites for OH^- ions within the coating during the electropolishing process [55,59]. The decrease in the total polarisation resistance $R_{ct} + R_{ad}$ after electropolishing also suggest that a passivation layer, which may reduce the material removal rate, does not naturally form during the electropolishing process and thus the material can be readily removed. Note that the total polarisation resistance is often used as a measure of corrosion resistance, where a higher polarisation resistance value represents a more robust passivation with a lower corrosion rate [50,51,53].

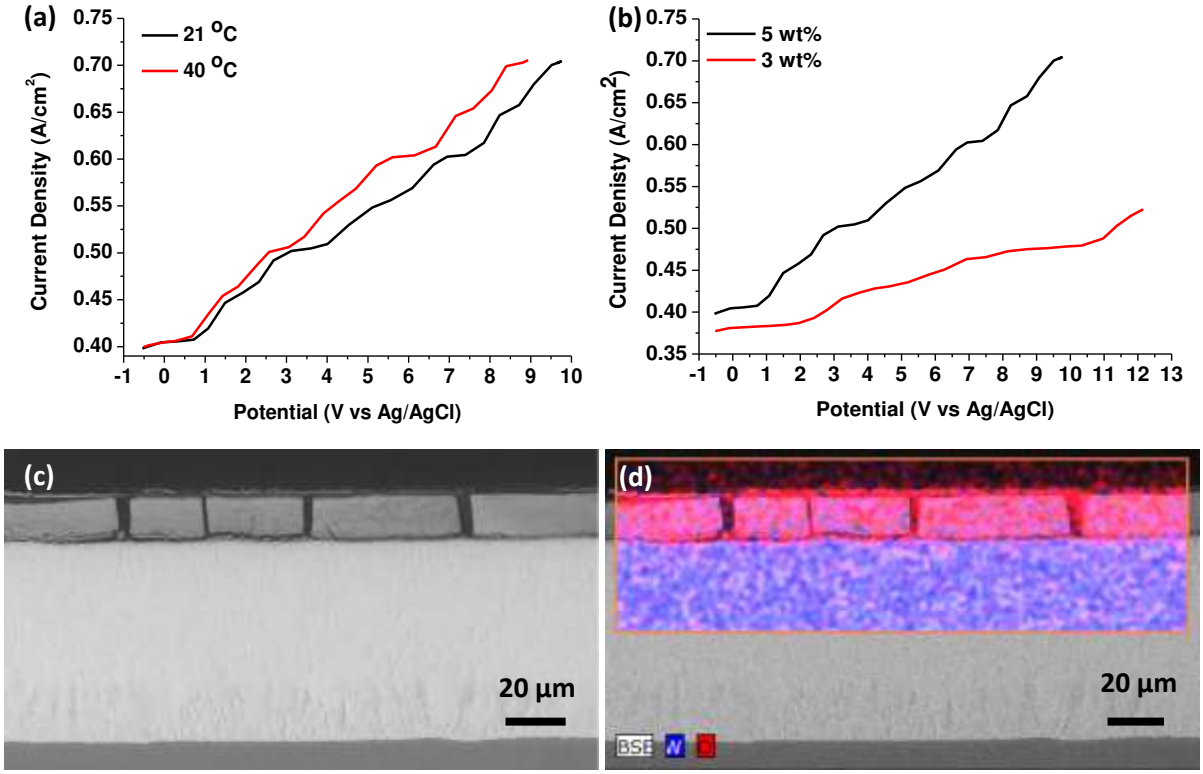


Figure 6: Anodic polarisation curves of W/WC in (a) 5 wt% NaOH electrolyte at temperature of 21 °C and 40 °C and (b) at 21 °C using electrolyte concentration of 5 wt% and 3 wt% NaOH. (c) SEM and (d) corresponding EDS maps of the cross-section showing the formation of WO_3 on W/WC coating under regime II conditions in 5 wt% NaOH solution at room temperature.

To further elucidate the parameter space of W/WC electropolishing in NaOH, the anodic polarisation is analysed under different electrolyte temperatures and concentrations. Note that anodic polarisation curves are typically segmented into four key regimes of etching (I), passivation (II), electropolishing (III), and gas evolution (IV). Here, the anodic polarisation curves are obtained by sweeping the applied potential at a sweep rate of 50 mV/s using an inter-electrode gap width of 15 cm. For 5 wt% NaOH at 21 °C (**Figure *6*a**), the increase in applied potential from 0 to 0.7 V vs Ag/AgCl does not significantly change the current density. It remains relatively stable at ~0.4 A/cm^2 due to the relatively low mass ion transport and the aforementioned high charge transfer resistance of the WO_x layer on the surface of W matrix [32,33,58]. The increase in potential from 0.7 to 3 V vs Ag/AgCl results in a linear increase in current density that indicates the etching (I) regime. In regime I, material dissolution starts to increase due to a higher mass transport of OH^- ions moving towards the anode and subsequent tungstate ions (WO_4^{2-}) being driven away from the surface of the workpiece (**Figure *7***) (Supporting information Figure SI 2). However, the rate of dissolution in regime I is still limited by the equilibrium between surface oxidation and chemical dissolution of WO_x on the surface of the workpiece [60]. This leads to the formation of valleys resembling etch pits on the W/WC coating (**Figure *2*b** and **Figure *3*b**). The passivation (II) regime is reached upon exceeding a potential of ~2.75 V vs Ag/AgCl. In regime II, the generated WO_x layer is at its thickest, providing a higher resistance to the applied potential and a subsequent stabilised current in the range of 2.75 – 4 V vs Ag/AgCl. The current is sufficiently high to generate excess of OH^- ions at the cathode that upon being transported toward the anode result in further oxidation of the WO_x layer into WO_3 (**Equation 1**) [32,33,58]. The formation of WO_3 layer with a thickness of up to 20 µm can be observed from the cross-sectional SEM image of the passivated samples (**Figure 6c-d**). This suggest that in regime II the surface passivation

(**Equation 1**) is more favourable than the oxide dissolution (**Equation 2**). At a higher applied potential of up to 8.7 V vs Ag/AgCl, material dissolution continues to occur where the electropolishing (III) regime is reached. Regime III is where the OH^- ions further oxidise the formed WO_3 at the anode surface into WO_4^{2-} ions (**Equation 2**). As the optimal surface finishing is achieved only in regime III, the dissolution of WO_3 into WO_4^{2-} ions can therefore be considered as the main mechanism for surface smoothening (**Figure *2*d** and **Figure *3*d**). Note that the formation of OH^- ions at the cathode is also accompanied by the formation of H_2 gas that evolves into bubbles **(Equation 3**). The level of noise in time dependent current density can be attributed to such formation and release of H_2 bubbles. The gas evolution regime (IV) is reached when a potential higher than 9 V vs Ag/AgCl is applied. In regime (IV), some of the excess OH^- ions are oxidised allowing the evolution of O_2 to take place. The presence of the evolution of O_2 bubbles on the surface of the workpiece leads to the formation of high-density pits.

Equation 1: $$W_{(s)} + 6OH^-_{(aq)} \rightarrow WO_{3\,(s)} + 3H_2O_{(aq)} + 6e^-$$

Equation 2: $$WO_{3\,(s)} + 2OH^-_{(aq)} \rightarrow WO^{2-}_{4(aq)} + H_2O_{(aq)}$$

Equation 3: $$6H_2O_{(aq)} + 6e^- \rightarrow 3H_{2\,(g)} + 6OH^-$$

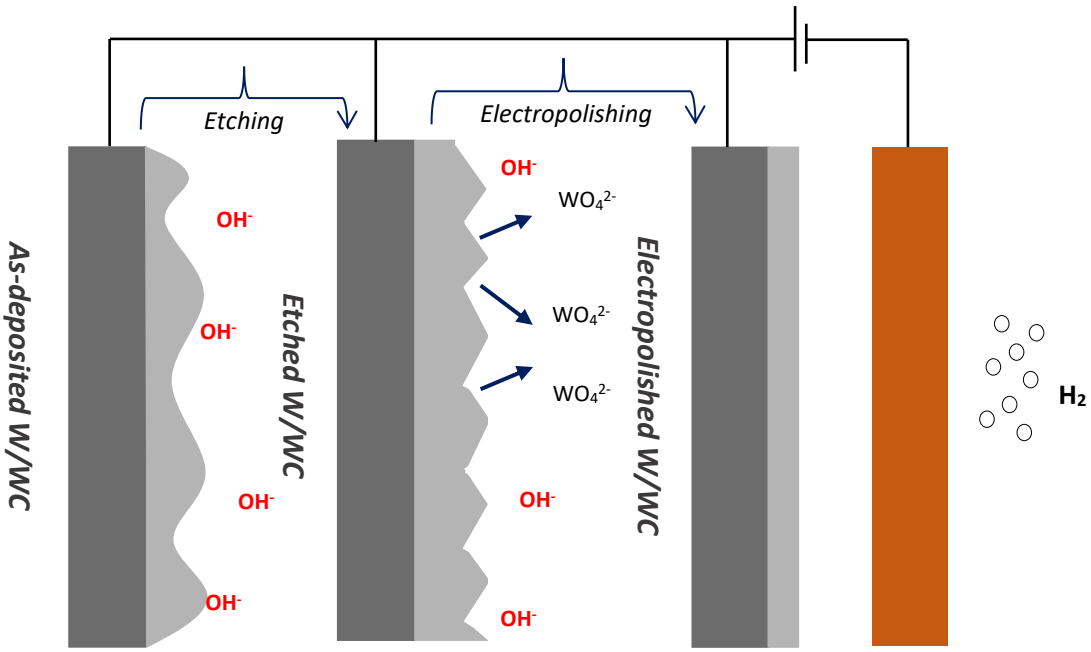


Figure 7: Schematic representation outlining the different electropolishing stages.

The effect of electrolyte temperature on the current density and electropolishing behaviour of W/WC in 5 wt% NaOH is analysed using an electrolyte temperature of 40 °C. Compared to the anodic polarisation curve obtained at 21 °C, that at 40 °C exhibit an overall higher current density with narrower etching, passivation, and limiting current regimes (**Figure *6*b**) where the electropolishing potential range at 40 °C is up to 2 V vs Ag/AgCl lower than that at 21 °C. The width of the limiting current plateau at 40 °C is similarly diminshed when compared to that at at 21 °C. This change in behaviour is attributed to the viscous film formed on the surface of the workpiece, where at high temperature a thin film is formed due to lower diffusion rates of electroyte ions. At a low temperature the diffusion of W ions away from the surface of the workpiece and OH^- ions toward the surface of the workpiece is slower. Consequently, the thickness of the viscous film is higher than that formed at

a 40 °C, resulting in a higher resistance and conseqnetly lower current density. At 40 °C, the ion solubility is higher, which allows reactions to occur at a faster rate but being also limited to a shorter potential range, thus requiring a better process control. This behaviour is in agreement with reported studies on the electropolishing of other metals [39,43,61–63].

The test using different electrolyte concentration shows that the 3 wt% NaOH results in a lower current density than the 5 wt% one (**Figure *8*b**). At 3 wt%, the passivation regime is more stable and spread over a wider voltage range. This behaviour is attributed to the formed WO_x being more stable at a lower NaOH concentration that results in a delay in its dissolution. Potentiostatic test at 7 V vs Ag/AgCl and 7.9 V vs Ag/AgCl using a 3 wt% NaOH electrolyte produces similar surface morphology to that using a 5 wt% NaOH electrolyte, where a mirror-like finish can still be achieved at a 7 V vs Ag/AgCl potential (**Figure *8*a**). In fact, the impact of electrolyte concentration on surface roughness is insignificant if the electropolishing is performed at 7–7.9 V vs Ag/AgCl for a short duration of 2 min. For both electolyte concentrations, the electropolished samples are observed to exhibit low surface roughness with Ra below 0.01 µm. Nevertheless, the W/WC coatings electropolished with 5 wt% NaOH have shown a relatively better surface finish than those with 3 wt% NaOH (**Table 2**). The morphology of the sample electropolised with 3 wt% NaOH shows that the surface is not completely flat with indication of some grains being selectively shallower than others due to preferential etching (**Figure *8*b**). NaOH electrolyte with a concentration of 5 wt% is therefore preferred in this study.

Table 2: Average change in surface roughness and standard deviation as a function of electrolyte concentration 2 mins tests.

Potential (V)	Electrolyte Concentration (3 wt%)		Electrolyte Concentration (5 wt%)	
	As-coated Ra (µm)	Electropolished Ra (µm)	As-coated Ra (µm)	Electropolished Ra (µm)
18	0.328 ± 0.036	0.084 ± 0.030	0.366 ± 0.073	0.064 ± 0.012
20	0.334 ± 0.029	0.063 ± 0.021	0.396 ± 0.065	0.051 ± 0.008

Furthermore, we observe that the time-dependent current density throughout the electropolishing process is more stable in 5 wt% than that in 3 wt% NaOH electrolyte. This allows a wide range of inter-electrode gaps to be used for electropolishing without excessively affecting the current density throughout the process. As expected, the average current density for W/WC in 5 wt% NaOH is higher than that in 3 wt% due to a lower ionic resistance from a higher number of available ions in the electrolytes. At a 15 cm inter-electrode gap, the current density in 5 wt% NaOH at an applied potential of 7 V vs Ag/AgCl is observed to follow a steady path of ~0.55 A/cm^2 with a very low level of noise (**Figure *8*c**). In contrast, the current density in 3 wt% NaOH for the same inter-electrode gap is observed at ~0.45 A/cm^2, but with a higher level of noise (**Figure *8*d**). The lower level of noise can be attributed to a more even distribution of H_2 bubbles released from the cathode. During the 120 seconds test, the spread of the current densities for various inter-electrode gaps (3-15 cm) at 5 wt% NaOH concentration was within 0.45-0.65 A/cm^2 range. At the 3 wt% NaOH concentration this varied between 0.5-0.6 A/cm^2 range. The lower spread of the current densities at 3 wt% NaOH concentration should help achieve more uniform electropolishing effect on non-flat workpiece, i.e., cylindrical

workpiece would have central area closer to the cathode but would still have similar current density as the peripheral areas further from the cathode.

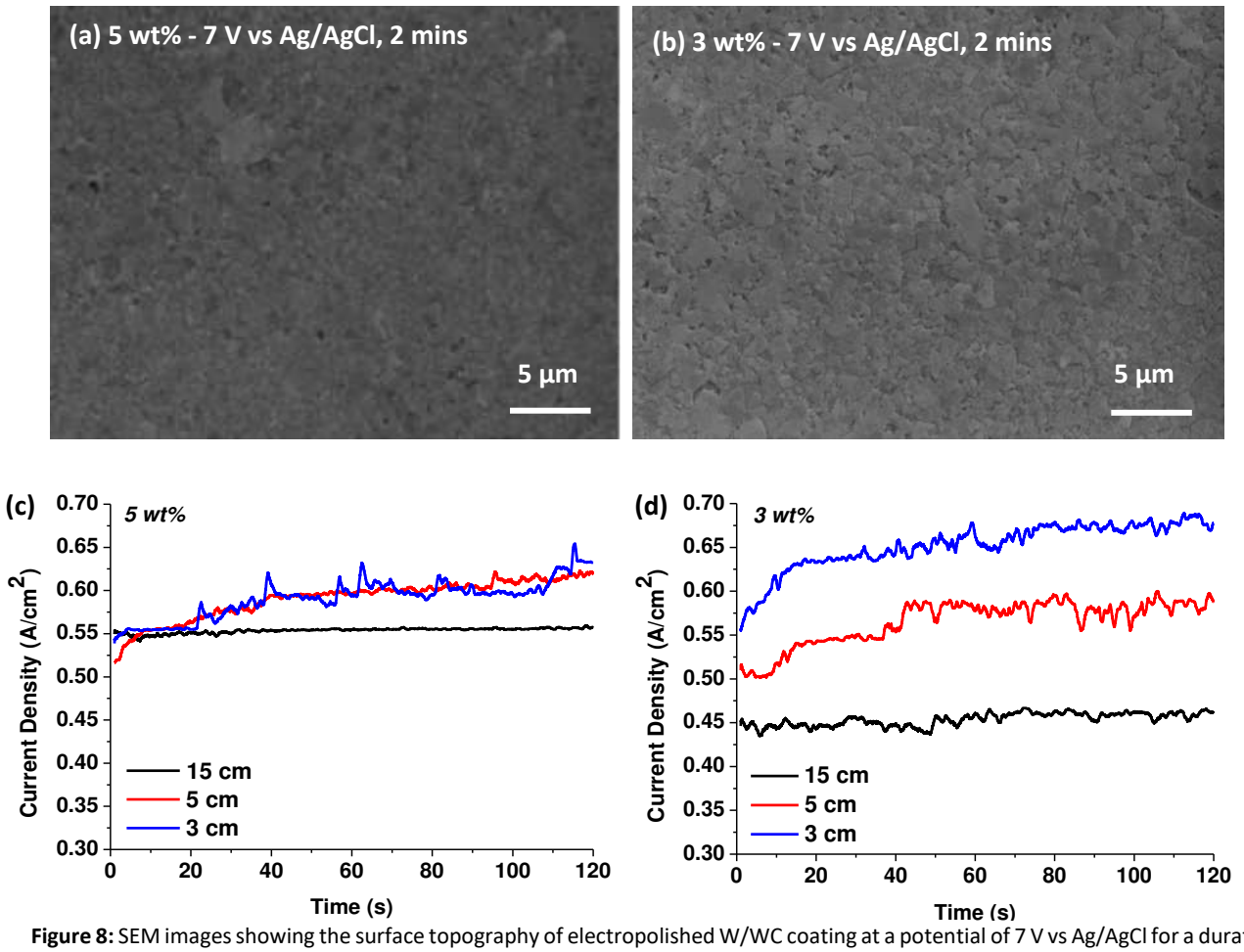


Figure 8: SEM images showing the surface topography of electropolished W/WC coating at a potential of 7 V vs Ag/AgCl for a duration of 2 mins in (a) 5 wt% and (b) 3 wt% NaOH. Variation in time-dependent current density obtained using inter-electrode gap of 3 cm, 5 cm, and 15 cm in (c) 5 wt% and (d) 3 wt% NaOH concentrations at 21 °C with a potential of 7 V vs Ag/AgCl.

For both concentrations, the magnitude of current density is observed to increase with the decrease in inter-electrode gap due to a decrease in ohmic resistance between both electrodes. For an inter-electrode gap of less than 15 cm, the current density is observed to increase with the increase in electropolishing time. For 5 wt% NaOH, the overall current density for samples electropolished with 3 and 5 cm inter-electrode gaps have shown similar transient behaviour, with the average current density increases from ~0.52 A/cm^2 to ~0.62 A/cm^2 within 2 mins of electropolishing. Nevertheless, the main difference is that at a 3 cm gap a higher occurrence of sharp increases and decreases in current density is observed from the 20 second mark onwards. Such sharp increases and drops in current density for small inter-electrode gaps can be attributed to the merging of many small H_2 bubbles into larger H_2 bubbles [29]. As these large bubbles escape the electrode gaps, they are immediately replaced by a fresh electrolyte solution that causes a surge in current density. The effect of H_2 bubbles evolution is amplified in a smaller electrode gap as they are not able to escape as freely into the bulk electrolyte as in a larger electrode gap. For 3 wt% NaOH, the current density transients for 3 and 5 cm inter-electrode gaps show similar characteristics, where the current density increases gradually for the first 20 s followed by a steady-state behaviour for the subsequent 15 seconds. Following this, a relatively high level of fluctuations is observed for the remaining duration of the

electropolishing due to the higher presence of H_2 bubbles. The average current density for 3 cm gap in 3 wt% NaOH increases from ~0.55 A/cm^2 to ~0.67 A/cm^2 within 2 mins of electropolishing, which is higher than that obtained in 5 wt% NaOH. Change in Ra as a function of interelectrode gap width and electrolyte concentration is shown in **Table 3**.

Table 3: Average change is surface roughness (Ra) and standard deviation as a function of the inter-electrode gap widths at potential of 7 V vs Ag/AgCl and 2 mins test time.

Inter-electrode gap width (cm)	Electrolyte concentration (3 wt%)		Electrolyte concentration (5 wt%)	
	As-coated Ra (µm)	Electropolished Ra (µm)	As-coated Ra (µm)	Electropolished Ra (µm)
3	0.59 ± 0.02	0.26 ± 0.001	0.59 ± 0.02	0.02 ± 0.001
5	0.59 ± 0.02	0.25 ± 0.001	0.59 ± 0.02	0.10 ± 0.03
15	0.30 ± 0.02	0.07 ± 0.02	0.37 ± 0.02	0.10 ± 0.01

Although a higher electrolyte concentration yields a more stable current density when a large inter-electrode gap is used, it does not necessarily mean a lower electrolyte concentration should be avoided. The rationale for using a lower electrolye concentration is based on the premise that a weaker electrochemical reaction would be involved due to a lower presence of OH^- ions and consequently a lower anodic dissolution of WO_x. A slow chemical reaction is particualrly important in this study to reduce the risk of affecting the coating integrity and have better control over the material removal rate. Due to the nature of the CVD process which induces thermal mismatch between the coating and the substrate, the W/WC coatings have high compressive residual stresses, coherency stresses, and intrinsic residual stresses. The coherency stress in the deposition of hard coating is associated to the substrate/coating interaction whereby the lattice spacing of the coating, which is different than that of the substrate, grows in the same direction as that of the substrate in an epitaxial way [64]. Intrinsic residual stresses refer to the stresses formed along grain boundaries during coating deposition through island coalescence, whereby different nucleated clusters are combined together to form a bulk body [64,65]. It was thus of primary importance to limit the chemical attack on the coatings so as not to allow large stress relaxations, which may ultimately affect the overall structural integrity of the coating and result in the formation of cracks or other defects.

Conclusions

In this study, we systematically investigate the parameter space underpinning the progressive changes in surface topography using various electrolyte concentrations, electrolyte temperatures, variable potential regimes, and inter-electrode gap widths. Through the use of 5 wt% NaOH electrolyte concentration, an average Ra surface finish of < 50 nm can be achieved within 5 mins by applying a potential of 7 V vs Ag/AgCl V. An increase in electrolyte temperature to 40 ^oC is found to negatively affect the overall surface finish of the coating due to the formation of a thinner and unstable viscous film restricting the electropolishing region to a small potential gap. Our results show a removal of

coating thickness of up to 18 µm can be achieved at a rate of 3.56 to 3.66 µm/minute. This suggests the suitability of electropolishing process for removing excess coating material, which is of importance for size correction and adherence to geometrical tolerances. EIS analysis further confirms that electropolishing process leads to surface transformation into a smooth and planar surface with homogeneous reaction sites. Electropolishing also results in the removal of charge barrier layer on the surface of W/WC coating that leads to lower resistances for charge transfer and adsorption of electroactive species. Inter-electrode gap of 15 cm is found to provide optimal surface finishing results when compared to 3 and 5 cm widths, where the current density transients are observed to be more uniform for 15 cm gaps due to better dispersion of hydrogen gas formed at the counter electrodes. Our EBSD analysis shows that preferential grain etching occurs along the {111} orientation, strongly suggesting that this orientation is electrochemically more active in alkaline solutions. Using the optimal processing parameters, we have been able to demonstrate the effectiveness of electropolishing as a noncontact machining technique to alter the initially matte surface texture of W/WC coatings into a mirror-like surface finish. The findings presented herein should be considered as a basis for further studies into surface finishing of other advanced materials, including hard coatings and difficult to process materials, to conform with the low surface roughness and stringent geometrical tolerance specifications of many extreme engineering applications.

Acknowledgement

AIA acknowledges partial support from EU Marie Sklodowska-Curie Actions (Grant No. 645725, FRIENDS2).

References:

1. Carbides, H.T.; Moskowitz, D.; Ford, M.J.; Humenik, M.; Company, F.M. *High-Strength Tungsten Carbides*; 1971;
2. R.K. Viswanadham, D.J.R. and J.G. *Science of Hard Materials*; Plenum Press: New York, 1984; Vol. 17;.
3. Cardarelli, F. Materials Handbook — a concise desktop reference. In *Materials & Design*; 2001; Vol. 22, p. 3069 ISBN 1852331682.
4. Prakash, L.; S, K.U.T.A. *Fundamentals and General Applications of Hardmetals*; Elsevier Ltd, 2014; Vol. 1; ISBN 9780080965277.
5. Micallef, C.; Zhuk, Y.N.; Wood, R.J.K. Galling resistance of nanostructured CVD tungsten/tungsten carbide coatings. *Surf. Topogr. Metrol. Prop.* **2019**, *7*, doi:10.1088/2051-672X/ab1535.
6. Wang, H.; Webb, T.; Bitler, J.W. Study of thermal expansion and thermal conductivity of cemented WC-Co composite. *Int. J. Refract. Met. Hard Mater.* **2015**, *49*, 170–177, doi:10.1016/j.ijrmhm.2014.06.009.
7. Wilson, B.L. The Effects of Abrasives on Electrical Submersible Pumps. *SPE Drill. Eng.* **1990**, 171–175.
8. Dyer, P.N.; Garg, D.; Pellman, M.A.; Sheridan, J.J. CVD Tungsten Carbide and Titanium Carbide Coatings for Aerospace Components. *SAE Trans.* **1989**, *98*, 64–70.

9. Goff, J.; Whelan, T. *The dynisco extrusion processors handbook*; DeLaney, D., Ed.; 2nd Editio.; Dynisco: Delano, Minnesota, 2000;

10. Kharlamov, Y.; Al-jawaheri, A.A.M. Dimensioning and tolerancing of coated parts. *TEKA. Comm. Mot. Energ. Agric.* **2014**, *14*, 105–114.

11. Phillips, Frank H., R.W. Finishing of tungsten carbide surfaces 1999, 1–12.

12. Kopac, J.; Krajnik, P. High-performance grinding - A review. *J. Mater. Process. Technol.* **2006**, *175*, 278–284, doi:10.1016/j.jmatprotec.2005.04.010.

13. ECHA Substances restricted under REACH Available online: https://echa.europa.eu/substances-restricted-under-reach (accessed on Aug 26, 2021).

14. Cebo, T.; Aria, A.I.; Dolan, J.A.; Weatherup, R.S.; Nakanishi, K.; Kidambi, P.R.; Divitini, G.; Ducati, C.; Steiner, U.; Hofmann, S.; et al. Chemical vapour deposition of freestanding sub-60 nm graphene gyroids Chemical vapour deposition of freestanding sub-60 nm graphene gyroids. *Appl. Phys. Lett.* **2017**, *111*.

15. Puglisi, R.A.; Bongiorno, C.; Caccamo, S.; Fazio, E.; Mannino, G.; Neri, F.; Scalese, S.; Spucches, D.; Magna, A. La Chemical Vapor Deposition Growth of Silicon Nanowires with Diameter Smaller Than 5 nm. *ACS Omega* **2019**, 7–11, doi:10.1021/acsomega.9b01488.

16. Nakanishi, K.; Aria, A.I.; Berwind, M.F.; Weatherup, R.S.; Eberl, C.; Hofmann, S.; Fleck, N.A. Acta Materialia Compressive behavior and failure mechanisms of freestanding and composite 3D graphitic foams. *Acta Mater.* **2018**, *159*, 187–196, doi:10.1016/j.actamat.2018.08.012.

17. Herth, E.; Rauch, J.Y. ICPECVD - Dielectric Thin - Films CMOS - Compatible : Trends in Eco - Friendly Deposition. *Int. J. Precis. Eng. Manuf. Technol.* **2021**, 25–27, doi:10.1007/s40684-021-00381-0.

18. Naeem, R.; Yahya, R.; Pandikumar, A.; Nay, H. Optical and optoelectronic properties of morphology and structure controlled ZnO , CdO and PbO thin films deposited by electric field directed aerosol assisted CVD. *J. Mater. Sci. Mater. Electron.* **2017**, *28*, 868–877, doi:10.1007/s10854-016-5601-3.

19. Kainz, C.; Schalk, N.; Tkadletz, M.; Mitterer, C.; Czettl, C. Surface & Coatings Technology Microstructure and mechanical properties of CVD TiN / TiBN multilayer coatings. *Surf. Coat. Technol.* **2019**, *370*, 311–319, doi:10.1016/j.surfcoat.2019.04.086.

20. Micallef, C.; Zhuk, Y.; Aria, A.I. Recent progress in precision machining and surface finishing of tungsten carbide hard composite coatings. *Coatings* **2020**, *10*, 1–36, doi:10.3390/coatings10080731.

21. Lohrengel, M.M.; Rataj, K.P.; Schubert, N.; Schneider, M.; Höhn, S.; Michaelis, A.; Hackert-Oschätzchen, M.; Martin, A.; Schubert, A. Electrochemical machining of hard metals - WC/Co as example. *Powder Metall.* **2014**, *57*, 21–30, doi:10.1179/1743290113Y.0000000062.

22. Hu, Y.N.; Zhou, H.; Liao, L.P.; Deng, H.B. Surface quality analysis of the electropolishing of cemented carbide. *J. Mater. Process. Technol.* **2003**, *139*, 253–256, doi:10.1016/S0924-0136(03)00230-9.

23. Chloé Rotty, Marie-Laure Dochea, Audrey Mandroyan, Jean-Yves Hihn, Ghislain Montavon, V.M. Electropolishing of Thermal Spray Coating and Laser Additive Manufacturing of 316L Stainless Steel in Strong Acidic Media. In Proceedings of the International conference on surface modification technologies (SMT30); 2016.

24. Lin, T.R.; Su, C.R. Experimental study of lapping and electropolishing of tungsten carbides. *Int.*

J. Adv. Manuf. Technol. **2008**, *36*, 715–723, doi:10.1007/s00170-006-0895-6.

25. García, J.; Collado Ciprés, V.; Blomqvist, A.; Kaplan, B. Cemented carbide microstructures: a review. *Int. J. Refract. Met. Hard Mater.* **2019**, *80*, 40–68, doi:10.1016/j.ijrmhm.2018.12.004.

26. Mukhopadhyay, A.; Basu, B. Recent developments on WC-based bulk composites. *J. Mater. Sci.* **2011**, *46*, 571–589, doi:10.1007/s10853-010-5046-7.

27. Zhuk, Y.N. Hardide™: Advanced nano-structured CVD coating. *Int. J. Microstruct. Mater. Prop.* **2007**, *2*, 90–98, doi:10.1504/IJMMP.2007.012942.

28. Wang, F. A comprehensive study on electrochemical polishing of tungsten. *Appl. Surf. Sci.* **2019**, *475*, 587–597, doi:10.1016/j.apsusc.2019.01.020.

29. Han, W.; Fang, F.Z. Investigation of electropolishing characteristics of tungsten in eco-friendly sodium hydroxide aqueous solution. *Adv. Manuf.* **2020**, *8*, 265–278, doi:10.1007/s40436-020-00309-y.

30. Davydov, A. Electrochemical dissolution of tungsten under pulsed conditions. *J. Appl. Electrochem.* **2014**, *27*, 351–354, doi:10.1023/A.

31. Ortiz, P.I.; Giordano, M.C.; Teijelo, M.L. Electrochemical behaviour of tungsten in alkaline media. *J. Electroanal. Chem. Interfacial Electrochem.* **1988**, *251*, 393–401, doi:10.1016/0022-0728(88)85199-4.

32. Weiss, H. V; Electro-, T.; Kelsey, G.S. The anodic oxidation of tungsten in aqueous base. *Electrochem. Sci. Technol.* **1977**, *124*, 814–819.

33. Tuvi, T.; Pašti, I.; Mentus, S. Tungsten electrochemistry in alkaline solutions - Anodic dissolution and oxygen reduction reaction. *Russ. J. Phys. Chem. A* **2011**, *85*, 2399–2405, doi:10.1134/S0036024411130322.

34. Oliver, M.R. Appendix: Pourbaix Diagrams. In *Springer Series in Materials Science Chemical-Mechanical Planarization of Semiconductor Materials*; 2004; Vol. 69, pp. 419–425.

35. Shangshang Wang, Jianbo Zhang, Oumaïma Gharbi, Vincent Vivier, M.G. and M.E.O. Electrochemical impedance spectroscopy. *Rev. Polarogr.* **2019**, *65*, 87–88, doi:10.5189/revpolarography.65.87.

36. Vargas Garcia, J.R.; Goto, T. Thermal barrier coatings produced by chemical vapor deposition. *Sci. Technol. Adv. Mater.* **2003**, *4*, 397–402, doi:10.1016/S1468-6996(03)00048-2.

37. Menéndez, A.; Sánchez, P.; Gómez, D. Deposition of Thin Films: PECVD Process. *Silicon Based Thin Film Sol. Cells* **2013**, 29–57, doi:10.2174/978160805518011301000 6.

38. Kashani, H.; Heydarzadeh Sohi, M.; Kaypour, H. Microstructural and physical properties of titanium nitride coatings produced by CVD process. *Mater. Sci. Eng. A* **2000**, *286*, 324–330, doi:10.1016/S0921-5093(00)00744-9.

39. Han, W.; Fang, F. Fundamental aspects and recent developments in electropolishing. *Int. J. Mach. Tools Manuf.* **2019**, *139*, 1–23, doi:10.1016/j.ijmachtools.2019.01.001.

40. Pendyala, P.; Bobji, M.S.; Madras, G. Evolution of surface roughness during electropolishing. *Tribol. Lett.* **2014**, *55*, 93–101, doi:10.1007/s11249-014-0336-x.

41. Holme, B.; Ljones, N.; Bakken, A.; Lunder, O.; Lein, J.E.; Vines, L.; Hauge, T.; Bauger, O.; Nisancioglu, K. Preferential Grain Etching of AlMgSi(Zn) Model Alloys. *J. Electrochem. Soc.* **2010**, *157*, C424, doi:10.1149/1.3496068.

42. Koroleva, E. V.; Thompson, G.E.; Skeldon, P.; Noble, B. Crystallographic dissolution of high purity aluminium. *Proc. R. Soc. A Math. Phys. Eng. Sci.* **2007**, *463*, 1729–1748, doi:10.1098/rspa.2007.1846.

43. Landolt, D. Fundamental aspects of electropolishing. *Electrochim. Acta* **1987**, *32*, 1–11, doi:10.1016/0013-4686(87)87001-9.

44. Palasantzas, G.; Backx, G.M.E.A. Roughness effects on the double-layer charge capacitance: The case of Helmholtz layer induced roughness attenuation. *Surf. Sci.* **2003**, *540*, doi:10.1016/S0039-6028(03)00877-X.

45. Birla Singh, M.; Kant, R. Theory of anomalous dynamics of electric double layer at heterogeneous and rough electrodes. *J. Phys. Chem. C* **2014**, *118*, 5122–5133, doi:10.1021/jp410999b.

46. Kerner, Z.; Pajkossy, T. Impedance of rough capacitive electrodes: The role of surface disorder. *J. Electroanal. Chem.* **1998**, *448*, 139–142, doi:10.1016/S0022-0728(98)00025-4.

47. Pajkossy, T. Impedance of rough capacitive electrodes. *J. Electroanal. Chem.* **1994**, *364*, 111–125, doi:10.1016/0022-0728(93)02949-I.

48. Song, H.K.; Hwang, H.Y.; Lee, K.H.; Dao, L.H. Effect of pore size distribution on the frequency dispersion of porous electrodes. *Electrochim. Acta* **2000**, *45*, 2241–2257, doi:10.1016/S0013-4686(99)00436-3.

49. Pajkossy, T. Impedance spectroscopy at interfaces of metals and aqueous solutions - Surface roughness, CPE and related issues. *Solid State Ionics* **2005**, *176*, 1997–2003, doi:10.1016/j.ssi.2004.06.023.

50. Ezhilselvi, V.; Nithin, J.; Balaraju, J.N.; Subramanian, S. The influence of current density on the morphology and corrosion properties of MAO coatings on AZ31B magnesium alloy. *Surf. Coatings Technol.* **2016**, *288*, 221–229, doi:10.1016/j.surfcoat.2016.01.040.

51. Gaona-Tiburcio, C.; Montoya-Rangel, M.; Cabral-Miramontes, J.A.; Estupiñan-López, F.; Zambrano-Robledo, P.; Cruz, R.O.; Chacón-Nava, J.G.; Baltazar-Zamora, M.Á.; Almeraya-Calderón, F. Corrosion resistance of multilayer coatings deposited by PVD on Inconel 718 using electrochemical impedance spectroscopy technique. *Coatings* **2020**, *10*, 1–11, doi:10.3390/COATINGS10060521.

52. Oldenburger, M.; Bedürftig, B.; Gruhle, A.; Grimsmann, F.; Richter, E.; Findeisen, R.; Hintennach, A. Investigation of the low frequency Warburg impedance of Li-ion cells by frequency domain measurements. *J. Energy Storage* **2019**, *21*, 272–280, doi:10.1016/j.est.2018.11.029.

53. Han, W.; Fang, F. Electropolishing of 316L stainless steel using sulfuric acid-free electrolyte. *J. Manuf. Sci. Eng. Trans. ASME* **2019**, *141*, 1–12, doi:10.1115/1.4044518.

54. Lasia, A. *Electrochemical impedance spectroscopy and its applications*; 1st ed.; Springer, New York, NY: Canada, 2007; Vol. 1; ISBN 9780444521903.

55. Alexander, C.L.; Tribollet, B.; Vivier, V.; Orazem, M.E. Contribution of Surface Distributions to Constant-Phase-Element (CPE) Behavior: 3. Adsorbed Intermediates. *Electrochim. Acta* **2017**, *251*, 99–108, doi:10.1016/j.electacta.2017.08.081.

56. Ter Heijne, A.; Schaetzle, O.; Gimenez, S.; Fabregat-Santiago, F.; Bisquert, J.; Strik, D.P.B.T.B.; Barrière, F.; Buisman, C.J.N.; Hamelers, H.V.M. Identifying charge and mass transfer resistances of an oxygen reducing biocathode. *Energy Environ. Sci.* **2011**, *4*, 5035–5043,

doi:10.1039/c1ee02131a.

57. Aria, A.I.; Gharib, M. Physicochemical characteristics and droplet impact dynamics of superhydrophobic carbon nanotube arrays. *Langmuir* **2014**, *30*, 6780–6790.

58. Anik, M.; Soc, J.E.; B-b, P.; Anik, M. Effect of pH on the anodic behavior of tungsten. *J. Electrochem. Soc.* **2002**, *149*, B224–B233, doi:10.1149/1.1471544.

59. Daniels, K.M.; Shetu, S.; Staser, J.; Weidner, J.; Williams, C.; Sudarshan, T.S.; Chandrashekhar, M. Mechanism of Electrochemical Hydrogenation of Epitaxial Graphene. *J. Electrochem. Soc.* **2015**, *162*, E37–E42, doi:10.1149/2.0191504jes.

60. Topalov, A.A.; Cherevko, S.; Zeradjanin, A.R.; Meier, J.C.; Katsounaros, I.; Mayrhofer, K.J.J. Towards a comprehensive understanding of platinum dissolution in acidic media. *Chem. Sci.* **2014**, *5*, 631–638, doi:10.1039/c3sc52411f.

61. Nath, C.; Rahman, M.; Neo, K.S. A study on the effect of tool nose radius in ultrasonic elliptical vibration cutting of tungsten carbide. *J. Mater. Process. Technol.* **2009**, *209*, 5830–5836, doi:10.1016/j.jmatprotec.2009.06.013.

62. Barnes, P.; Savva, A.; Dixon, K.; Bull, H.; Rill, L.; Karsann, D.; Croft, S.; Schimpf, J.; Xiong, H. Electropolishing valve metals with a sulfuric acid-methanol electrolyte at low temperature. *Surf. Coatings Technol.* **2018**, *347*, 150–156, doi:10.1016/j.surfcoat.2018.04.082.

63. Landolt, D.; Chauvy, P.F.; Zinger, O. Electrochemical micromachining, polishing and surface structuring of metals: Fundamental aspects and new developments. *Electrochim. Acta* **2003**, *48*, 3185–3201, doi:10.1016/S0013-4686(03)00368-2.

64. Cammarata, R.C.; Trimble, T.M.; Srolovitz, D.J. Surface stress model for intrinsic stresses in thin films. *J. Mater. Res.* **2000**, *15*, 2468–2474, doi:10.1557/JMR.2000.0354.

65. Sheldon, B.W.; Lau, K.H.A.; Rajamani, A. Intrinsic stress, island coalescence, and surface roughness during the growth of polycrystalline films. *J. Appl. Phys.* **2001**, *90*, doi:10.1063/1.1412577.



https://dspace.org/

Rapid surface finishing of chemical vapour deposited tungsten carbide hard coatings by electropolishing

Micallef, Christian; Chiu, Cheng-Wei; Zhuk, Yuri; Aria, Adrianus Indrat

2021-11-15
Elsevier
https://doi.org/10.1016/j.surfcoat.2021.127900
Micallef C, Chiu C-W, Zhuk Y, Aria AI. (2021) Rapid surface finishing of chemical vapour deposited tungsten carbide hard coatings by electropolishing. Surface and Coatings Technology, Volume 428, December 2021, Article number 127900

Downloaded from a DSpace repository. https://dspace.org/